Research Article | Vol. 7, No. 11 | 1 Nov 2016 | BIOMEDICAL OPTICS EXPRESS 4554
Biomedical Optics EXPRESS

Photoreceptor disc shedding in the living human eye

OMER P. KOCAOGLU,[1] ZHUOLIN LIU,[1] FURU ZHANG,[1] KAZUHIRO KUROKAWA,[1] RAVI S. JONNAL,[2] AND DONALD T. MILLER[1,*]

[1]*School of Optometry, Indiana University, Bloomington, IN 47405, USA*
[2]*Department of Ophthalmology & Vision Science, University of California, Davis, CA 95616, USA*
[*]*dtmiller@indiana.edu*

Abstract: Cone photoreceptors undergo a daily cycle of renewal and shedding of membranous discs in their outer segments (OS), the portion responsible for light capture. These physiological processes are fundamental to maintaining photoreceptor health, and their dysfunction is associated with numerous retinal disease. While both processes have been extensively studied in animal models and postmortem eyes, little is known about them in the living eye, in particular human. In this study, we report discovery of the optical signature associated with disc shedding using a method based on adaptive optics optical coherence tomography (AO-OCT) in conjunction with post-processing methods to track and monitor individual cone cells in 4D. The optical signature of disc shedding is characterized by an abrupt transient loss in the cone outer segment tip (COST) reflection followed by its return that is axially displaced anteriorly. Using this signature, we measured the temporal and spatial properties of shedding events in three normal subjects. Average duration of the shedding event was 8.8 ± 13.4 minutes, and average length loss of the OS was 2.1 μm (7.0% of OS length). Prevalence of cone shedding was highest in the morning (14.3%) followed by the afternoon (5.7%) and evening (4.0%), with load distributed across the imaged patch. To the best of our knowledge these are the first images of photoreceptor disc shedding in the living retina.

OCIS codes: (170.4500) Optical coherence tomography; (110.1080) Active or adaptive optics; (330.5310) Vision - photoreceptors; (330.4300) Vision system - noninvasive assessment; (330.7331) Visual optics, receptor optics; (170.4470) Ophthalmology.

References and links

1. L. Ruggiero and S. C. Finnemann, *Rhythmicity of the Retinal Pigment Epithelium*, Retina and Circadian Rhythms (Springer Series in Vision Research, 2014), Vol. 1.
2. B. M. Kevany and K. Palczewski, "Phagocytosis of retinal rod and cone photoreceptors," Physiology (Bethesda) **25**(1), 8–15 (2010).
3. C. H. Sung and J. Z. Chuang, "The cell biology of vision," J. Cell Biol. **190**(6), 953–963 (2010).
4. A. Gal, Y. Li, D. A. Thompson, J. Weir, U. Orth, S. G. Jacobson, E. Apfelstedt-Sylla, and D. Vollrath, "Mutations in MERTK, the human orthologue of the RCS rat retinal dystrophy gene, cause retinitis pigmentosa," Nat. Genet. **26**(3), 270–271 (2000).
5. S. van Soest, A. Westerveld, P. T. V. M. de Jong, E. M. Bleeker-Wagemakers, and A. A. B. Bergen, "Retinitis pigmentosa: Defined from a molecular point of view," Surv. Ophthalmol. **43**(4), 321–334 (1999).
6. S. Y. Kim, "Retinal phagocytes in age-related macular degeneration," Macrophage (Houst) **2**(1), e698 (2015).
7. C. C. Yu, E. F. Nandrot, Y. Dun, and S. C. Finnemann, "Dietary antioxidants prevent age-related retinal pigment epithelium actin damage and blindness in mice lacking αvβ5 integrin," Free Radic. Biol. Med. **52**(3), 660–670 (2012).
8. S. Zacchigna, H. Oh, M. Wilsch-Bräuninger, E. Missol-Kolka, J. Jászai, S. Jansen, N. Tanimoto, F. Tonagel, M. Seeliger, W. B. Huttner, D. Corbeil, M. Dewerchin, S. Vinckier, L. Moons, and P. Carmeliet, "Loss of the Cholesterol-Binding Protein Prominin-1/CD133 Causes Disk Dysmorphogenesis and Photoreceptor Degeneration," J. Neurosci. **29**(7), 2297–2308 (2009).
9. Z. Yang, Y. Chen, C. Lillo, J. Chien, Z. Yu, M. Michaelides, M. Klein, K. A. Howes, Y. Li, Y. Kaminoh, H. Chen, C. Zhao, Y. Chen, Y. T. Al-Sheikh, G. Karan, D. Corbeil, P. Escher, S. Kamaya, C. Li, S. Johnson, J. M. Frederick, Y. Zhao, C. Wang, D. J. Cameron, W. B. Huttner, D. F. Schorderet, F. L. Munier, A. T. Moore, D. G. Birch, W. Baehr, D. M. Hunt, D. S. Williams, and K. Zhang, "Mutant prominin 1 found in patients with macular degeneration disrupts photoreceptor disk morphogenesis in mice," J. Clin. Invest. **118**(8), 2908–2916 (2008).

#274076 http://dx.doi.org/10.1364/BOE.7.004554
Journal © 2016 Received 22 Aug 2016; revised 19 Sep 2016; accepted 19 Sep 2016; published 13 Oct 2016

Biomedical Optics EXPRESS

10. M. Koike, M. Shibata, Y. Ohsawa, H. Nakanishi, T. Koga, S. Kametaka, S. Waguri, T. Momoi, E. Kominami, C. Peters, K. Figura, P. Saftig, and Y. Uchiyama, "Involvement of two different cell death pathways in retinal atrophy of cathepsin D-deficient mice," Mol. Cell. Neurosci. **22**(2), 146–161 (2003).
11. R. W. Young and D. Bok, "Participation of the retinal pigment epithelium in the rod outer segment renewal process," J. Cell Biol. **42**(2), 392–403 (1969).
12. R. W. Young, "The renewal of photoreceptor cell outer segments," J. Cell Biol. **33**(1), 61–72 (1967).
13. D. H. Anderson, S. K. Fisher, and R. H. Steinberg, "Mammalian cones: disc shedding, phagocytosis, and renewal," Invest. Ophthalmol. Vis. Sci. **17**(2), 117–133 (1978).
14. R. H. Steinberg, I. Wood, and M. J. Hogan, "Pigment epithelial ensheathment and phagocytosis of extrafoveal cones in human retina," Philos. Trans. R. Soc. Lond. B Biol. Sci. **277**(958), 459–471 (1977).
15. D. H. Anderson and S. K. Fisher, "The photoreceptors of diurnal squirrels: outer segment structure, disc shedding, and protein renewal," J. Ultrastruct. Res. **55**(1), 119–141 (1976).
16. D. H. Anderson and S. K. Fisher, "Disc shedding in rodlike and conelike photoreceptors of tree squirrels," Science **187**(4180), 953–955 (1975).
17. R. S. Jonnal, J. R. Besecker, J. C. Derby, O. P. Kocaoglu, B. Cense, W. Gao, Q. Wang, and D. T. Miller, "Imaging outer segment renewal in living human cone photoreceptors," Opt. Express **18**(5), 5257–5270 (2010).
18. M. Pircher, J. S. Kroisamer, F. Felberer, H. Sattmann, E. Götzinger, and C. K. Hitzenberger, "Temporal changes of human cone photoreceptors observed in vivo with SLO/OCT," Biomed. Opt. Express **2**(1), 100–112 (2011).
19. R. S. Jonnal, O. P. Kocaoglu, Q. Wang, S. Lee, and D. T. Miller, "Phase-sensitive imaging of the outer retina using optical coherence tomography and adaptive optics," Biomed. Opt. Express **3**(1), 104–124 (2012).
20. R. F. Cooper, A. M. Dubis, A. Pavaskar, J. Rha, A. Dubra, and J. Carroll, "Spatial and temporal variation of rod photoreceptor reflectance in the human retina," Biomed. Opt. Express **2**(9), 2577–2589 (2011).
21. A. Pallikaris, D. R. Williams, and H. Hofer, "The reflectance of single cones in the living human eye," Invest. Ophthalmol. Vis. Sci. **44**(10), 4580–4592 (2003).
22. Z. Liu, O. P. Kocaoglu, and D. T. Miller, "In-the-plane design of an off-axis ophthalmic adaptive optics system using toroidal mirrors," Biomed. Opt. Express **4**(12), 3007–3029 (2013).
23. O. P. Kocaoglu, T. L. Turner, Z. Liu, and D. T. Miller, "Adaptive optics optical coherence tomography at 1 MHz," Biomed. Opt. Express **5**(12), 4186–4200 (2014).
24. B. A. Shafer, J. E. Kriske, O. P. Kocaoglu, T. L. Turner, Z. Liu, J. J. Lee, and D. T. Miller, "Adaptive-Optics Optical Coherence Tomography Processing Using a Graphics Processing Unit," Conf. Proc. IEEE Eng. Med. Biol. Soc. **2014**, 3877–3880 (2014).
25. ANSI Z136, "Safe use of lasers," Laser Institute of America (2014).
26. K. P. Wright, Jr., A. W. McHill, B. R. Birks, B. R. Griffin, T. Rusterholz, and E. D. Chinoy, "Entrainment of the human circadian clock to the natural light-dark cycle," Curr. Biol. **23**(16), 1554–1558 (2013).
27. J. F. Duffy and K. P. Wright, Jr., "Entrainment of the human circadian system by light," J. Biol. Rhythms **20**(4), 326–338 (2005).
28. C. Gronfier, K. P. Wright, Jr., R. E. Kronauer, and C. A. Czeisler, "Entrainment of the human circadian pacemaker to longer-than-24-h days," Proc. Natl. Acad. Sci. U.S.A. **104**(21), 9081–9086 (2007).
29. B. Middleton, B. M. Stone, and J. Arendt, "Human circadian phase in 12:12 h, 200: <8 lux and 1000: <8 lux light-dark cycles, without scheduled sleep or activity," Neurosci. Lett. **329**(1), 41–44 (2002).
30. Z. Liu, O. P. Kocaoglu, T. L. Turner, and D. T. Miller, "Modal content of living human cone photoreceptors," Biomed. Opt. Express **6**(9), 3378–3404 (2015).
31. O. P. Kocaoglu, R. D. Ferguson, R. S. Jonnal, Z. Liu, Q. Wang, D. X. Hammer, and D. T. Miller, "Adaptive optics optical coherence tomography with dynamic retinal tracking," Biomed. Opt. Express **5**(7), 2262–2284 (2014).
32. Z. Liu, O. P. Kocaoglu, and D. T. Miller, "3D Imaging of Retinal Pigment Epithelial Cells in the Living Human Retina," Invest. Ophthalmol. Vis. Sci. **57**(9), OCT533 (2016).
33. R. S. Jonnal, O. P. Kocaoglu, R. J. Zawadzki, S. H. Lee, J. S. Werner, and D. T. Miller, "The cellular origins of the outer retinal bands in optical coherence tomography images," Invest. Ophthalmol. Vis. Sci. **55**(12), 7904–7918 (2014).
34. R. S. Jonnal, O. P. Kocaoglu, R. J. Zawadzki, Z. Liu, D. T. Miller, and J. S. Werner, "A Review of Adaptive Optics Optical Coherence Tomography: Technical Advances, Scientific Applications, and the Future," Invest. Ophthalmol. Vis. Sci. **57**(9), OCT51–OCT68 (2016).
35. S. K. Fisher, B. A. Pfeffer, and D. H. Anderson, "Both rod and cone disc shedding are related to light onset in the cat," Invest. Ophthalmol. Vis. Sci. **24**(7), 844–856 (1983).
36. D. H. Anderson, S. K. Fisher, P. A. Erickson, and G. A. Tabor, "Rod and cone disc shedding in the rhesus monkey retina: a quantitative study," Exp. Eye Res. **30**(5), 559–574 (1980).
37. M. M. LaVail, "Kinetics of rod outer segment renewal in the developing mouse retina," J. Cell Biol. **58**(3), 650–661 (1973).
38. M. M. LaVail, "Photoreceptor characteristics in congenic strains of RCS rats," Invest. Ophthalmol. Vis. Sci. **20**(5), 671–675 (1981).
39. N. Buyukmihci and G. D. Aguirre, "Rod disc turnover in the dog," Invest. Ophthalmol. **15**(7), 579–584 (1976).
40. G. Aguirre and L. Andrews, "Nomarski evaluation of rod outer segment renewal in a hereditary retinal degeneration. Comparison with autoradiographic evaluation," Invest. Ophthalmol. Vis. Sci. **28**(7), 1049–1058 (1987).

Biomedical Optics EXPRESS

41. R. W. Young, "The renewal of rod and cone outer segments in the rhesus monkey," J. Cell Biol. **49**(2), 303–318 (1971).
42. S. K. Fisher, B. A. Pfeffer, and D. H. Anderson, "Both rod and cone disc shedding are related to light onset in the cat," Invest. Ophthalmol. Vis. Sci. **24**(7), 844–856 (1983).
43. R. W. Young, "The daily rhythm of shedding and degradation of rod and cone outer segment membranes in the chick retina," Invest. Ophthalmol. Vis. Sci. **17**(2), 105–116 (1978).
44. W. T. O'Day and R. W. Young, "Rhythmic daily shedding of outer-segment membranes by visual cells in the goldfish," J. Cell Biol. **76**(3), 593–604 (1978).
45. R. W. Young, "The daily rhythm of shedding and degradation of cone outer segment membranes in the lizard retina," J. Ultrastruct. Res. **61**(2), 172–185 (1977).
46. N. F. Johnson, "Phagocytosis in the normal and ischaemic retinal pigment epithelium of the rabbit," Exp. Eye Res. **20**(2), 97–107 (1975).
47. M. M. LaVail, "Circadian nature of rod outer segment disc shedding in the rat," Invest. Ophthalmol. Vis. Sci. **19**(4), 407–411 (1980).
48. A. I. Goldman, P. S. Teirstein, and P. J. O'Brien, "The role of ambient lighting in circadian disc shedding in the rod outer segment of the rat retina," Invest. Ophthalmol. Vis. Sci. **19**(11), 1257–1267 (1980).
49. R. J. Mullen and M. M. LaVail, "Inherited retinal dystrophy: primary defect in pigment epithelium determined with experimental rat chimeras," Science **192**(4241), 799–801 (1976).
50. S. Basinger, R. Hoffman, and M. Matthes, "Photoreceptor shedding is initiated by light in the frog retina," Science **194**(4269), 1074–1076 (1976).
51. A. Krigel, M. P. Felder-Schmittbuhl, and D. Hicks, "Circadian-clock driven cone-like photoreceptor phagocytosis in the neural retina leucine zipper gene knockout mouse," Mol. Vis. **16**, 2873–2881 (2010).
52. C. Bobu and D. Hicks, "Regulation of retinal photoreceptor phagocytosis in a diurnal mammal by circadian clocks and ambient lighting," Invest. Ophthalmol. Vis. Sci. **50**(7), 3495–3502 (2009).
53. J. H. Immel and S. K. Fisher, "Cone photoreceptor shedding in the tree shrew (Tupaia belangerii)," Cell Tissue Res. **239**(3), 667–675 (1985).
54. G. W. Balkema, Jr. and A. H. Bunt-Milam, "Cone outer segment shedding in the goldfish retina characterized with the 3H-fucose technique," Invest. Ophthalmol. Vis. Sci. **23**(3), 319–331 (1982).
55. G. A. Tabor, S. K. Fisher, and D. H. Anderson, "Rod and cone disc shedding in light-entrained tree squirrels," Exp. Eye Res. **30**(5), 545–557 (1980).
56. K. O. Long, S. K. Fisher, R. N. Fariss, and D. H. Anderson, "Disc shedding and autophagy in the cone-dominant ground squirrel retina," Exp. Eye Res. **43**(2), 193–205 (1986).
57. L. Ruggiero, M. P. Connor, J. Chen, R. Langen, and S. C. Finnemann, "Diurnal, localized exposure of phosphatidylserine by rod outer segment tips in wild-type but not Itgb5-/- or Mfge8-/- mouse retina," Proc. Natl. Acad. Sci. U.S.A. **109**(21), 8145–8148 (2012).
58. G. Staurenghi, S. Sadda, U. Chakravarthy, and R. F. Spaide; International Nomenclature for Optical Coherence Tomography (IN•OCT) Panel, "Proposed lexicon for anatomic landmarks in normal posterior segment spectral-domain optical coherence tomography: the IN•OCT consensus," Ophthalmology **121**(8), 1572–1578 (2014).

1. Introduction

Photoreceptors undergo daily renewal and shedding of outer segment (OS) discs. These physiological mechanisms enable the OS to maintain a constant length while replacing components that have accumulated toxic photo-oxidative compounds. Renewal is the continual assembly of new membranous discs at the proximal end of the OS, which elongates the OS by a couple of microns each day. This new growth is offset by shedding, a discrete, diurnal event in which small packets of discs are pruned from the distal end of the OS. The disc packets are subsequently eliminated by phagocytosis by the underlying retinal pigment epithelium (RPE). Collectively, these mechanisms of renewal and shedding maintain health of the outer retina. Dysfunction at any stage or loss in synchronization (e.g., loss of diurnal rhythm) can lead to photoreceptor and RPE dystrophy, and ultimately blindness. Anomalies in these mechanisms have been implicated in numerous retinal diseases [1, 2], including retinitis pigmentosa (RP) [3–5] and age related macular degeneration (AMD) [6–10], and are thus of significant clinical interest.

OS renewal and shedding were first discovered in rods by Young in the late 1960s using radioactive amino acids [11, 12] and then later in cones [13–16], and have since been extensively studied in animal models in postmortem eyes. Today, much is known about the diurnal rhythm and circadian control of renewal and shedding. In addition, the complex molecular and signaling pathways that underpin these processes are beginning to be elucidated in detail. But all of these advancements have occurred almost exclusively in animal models using postmortem eyes. How these translate to the living retina and to humans, where

Biomedical Optics EXPRESS

this knowledge can make its largest impact for improved diagnostics and therapeutics, remain major obstacles.

Only recently has renewal been measured in the living eye [17] and confirmed in subsequent imaging studies [18, 19]. These observations were all made in humans using high-resolution adaptive optics (AO) imaging systems that corrected aberrations of the eye and permitted visualization of individual cone photoreceptors. However even with AO-assisted systems, photoreceptor shedding has proven elusive [17–21].

In this study, we present what is to the best of our knowledge the first images of photoreceptor disc shedding in the living retina of any species. This was achieved in the human eye using a research-grade optical coherence tomography system equipped with adaptive optics (AO-OCT) and enabled us to characterize the optical signature of cone shedding. Critical to our method were custom post-processing algorithms to track and monitor over hours the 3D reflectance profile of individual cones. We substantiated our observations with quantitative analyses of the spatial and temporal properties of cone shedding dynamics in three normal subjects. These first experiments establish a clear path for further investigation of photoreceptor shedding, which are now underway in our laboratory.

2. Materials and methods

The methods section is divided in three parts. Section 2.1 presents the high-resolution AO-OCT system used to image cone photoreceptors. The experimental procedures and subject information are described in Section 2.2, and the post-processing steps used to extract photoreceptor disc shedding information from AO-OCT volume images are described in Section 2.3.

2.1. Description of the Indiana AO-OCT system

The AO-OCT system used for this study was previously described by Liu *et al.*, 2013 [22] and Kocaoglu *et al.*, 2014 [23]. In short, the AO-OCT system is composed of four optical channels (source, sample, reference, and detection) that are connected by a 2×2 780HP fiber coupler with 90/10 splitting ratio. The source arm contains a superluminescent diode laser (SLD, Superlum, Ireland) with central wavelength at λ_c = 785 nm and bandwidth of $\Delta\lambda$ = 47 nm, which provides a theoretical axial resolution of 4.2 μm in retinal tissue (n = 1.38). The sample arm consists of active elements (X and Y galvanometer scanners, a custom Shack-Hartman wave front sensor, a deformable mirror (DM97, ALPAO, France)), and passive elements (numerous mirror-based telescopes to conjugate the active components to the eye pupil). Astigmatism generated at both retinal and pupil conjugate planes due to the off-axis use of spherical mirrors was corrected with three customized toroidal mirrors. This solution preserves the global XY coordinate system [22]. The AO system dynamically measured and corrected ocular aberrations, and its performance was assessed in terms of the residual wavefront root-mean-square (RMS) error as well as the quality of the real-time *en face* retinal AO-OCT images [24]. The detection channel contains a custom quad-spectrometer consisting of four high speed spectrometers based on CMOS line-scan cameras that operate at 2 μs exposures at their fastest setting. A 1×4 fiber-based optical switch assembly directs the light to the four spectrometers. The system is scalable enabling one-camera (62.5% duty cycle), two-camera (100% duty cycle), and four-camera (100% duty cycle) modes that acquire A-scans at 250 KHz, 500 KHz, and 1MHz speeds, respectively.

2.2. Experimental protocol

Subjects: Three healthy subjects free of ocular disease were recruited for the cone shedding experiment. Subjects had best corrected visual acuity of 20/20 or better. Table 1 summarizes subject information relevant for the study. Eye lengths were measured with IOLMaster (Zeiss, Oberkochen, Germany). The AO-OCT light power incident on the subject's cornea was at or below 400 μW and within safe limits defined by ANSI [25] for the experimental protocol

Biomedical Optics EXPRESS

described here. All procedures on the subjects adhered to the tenets of the Declaration of Helsinki and were approved by the Institutional Review Board of Indiana University. Written informed consent was obtained after the nature and possible risks of the study were explained.

Table 1. Subject information.

Subject #	Age (y)	Gender	Spherical equiv. refractive error (D)	Axial length (mm)	Imaged Retinal Eccentricity (from fovea)
1	36	M	–3	26.1	2° Temporal
2	48	M	–2.5	25.4	3° Temporal
3	32	F	0	23.7	3° Temporal

Subject entrainment: Subjects maintained a 16/8 hour awake/sleep (light/dark) cycle for several days preceding the imaging experiments, in this way establishing light entrainment [26, 27]. Subjects were instructed to maintain daily routines of work, school, and additional activities within the 16 hour awake period. Likewise during the sleep cycle, subjects were instructed to avoid light exposure, in particular that above 100 lux [28, 29]. Start of the sleep period was self-selected.

Image acquisition protocol: Prior to each imaging session, the right eye was cyclopleged and dilated with one drop of Tropicamide 0.5% and maintained with an additional drop one hour later. The eye and head were aligned and stabilized using a bite bar mounted to a motorized XYZ translation stage. Table 2 summarizes the image acquisition parameters. Settings of a few acquisition parameters were refined between subjects in order to improve the efficiency of the experiment, e.g., by increasing imaging speed. These refinements were deemed unlikely to impact the experiment's independent and dependent variables (namely, time of day and the disappearance of cone outer segment tips (COST), respectively) and had no effect on subsequent analytical methods. At the highest A-line acquisition rate (500 KHz), the cone inner-outer segment junction (IS/OS) and COST were clearly visible and quantifiable, while intra-frame eye motion was minimized.

Table 2. Image acquisition parameters.

Parameters	Subject #1	Subject #2	Subject #3
A-line acquisition rate	500 KHz	250 KHz	500 KHz
A-line sampling	1 μm/px	1 μm/px	1 μm/px
# of A-lines per B-scan	450	270	300
# of B-scans per volume	450	220	300
B-scan acquisition rate	1.1 KHz	0.93 KHz	1.7 KHz
# of volumes per video	10	10	15
Volume video duration	4.4 s	2.6 s	3.1 s
AO-OCT image FOV	1.5° × 1.5°	0.9° × 0.7°	1° × 1°
Imaging frequency and duration	Every 3 min for 90 min	Every 3 min for 90 min	Every 3 min for 90 min
# of sessions	Morning	Morning, afternoon, evening	Morning, afternoon, evening

Each imaging session lasted 90 minutes with volume videos acquired every three minutes. For subject #1, one 90-minute session was conducted in the morning starting one hour after the subject's light/awake cycle began (~8-9:30 AM). For subject #2, the 90-minute imaging session was repeated at three different times of day, first in the morning starting one hour after the beginning of subject's light/awake cycle (~9-10:30 AM), second in the afternoon (3-4:30 PM), and last in the evening (9-10:30 PM), which occurred after dark onset. The three sessions were imaged on different days to avoid possible disruption of the subject's daily rhythm by preceding sessions. Subject #2 was entrained for each session. Subject #3 repeated the imaging protocol of subject #2, but with the three sessions on the same day.

Empirically we found a 3-minute imaging interval sufficiently narrow for catching the transient changes in the cones' reflectance associated with disc shedding. Because all cones are expected to shed regardless of location, we chose to image retinal eccentricities of 2° and 3° based on other criteria. Cones are readily distinguishable at these eccentricities with our

Biomedical Optics EXPRESS

AO-OCT system and exhibit single mode waveguide properties [30], which simplifies post processing. In addition, the relatively small diameter of the cones enabled hundreds of cones to fit even within the smallest AO-OCT volume size used (0.9°×0.7°, or approximately 270×220 μm^2 using a conversion of 300 μm/°). At each time point, an AO-OCT volume video was recorded and consisted of at least 10 volumes. From each video, a single volume was selected for analysis, on the basis of minimal eye motion artifacts and maximum *en face* overlap with volumes selected for other time points. Subsequent analysis was limited to these selected volumes.

2.3. Post processing: registration of time-lapse images

In order to follow single cones over the course of the experiment, the selected volumes were co-registered in three dimensions using modified versions of previously described algorithms [19, 31, 32]. Features of interest (IS/OS and COST) were labeled in each A-line using cross-correlation with a gross model of retinal reflectance, and these labels were used to produce high-contrast *en face* projections of those layers (see, e.g., Fig. 1(a)). These projections permitted lateral registration of volumes using a strip-wise algorithm [19]. Cones were automatically detected, and those present in all volumes (i.e., never missing from the FOV due to eye movements) were used for analysis.

In order to detect and quantify shedding events, several visualization steps were used. First, the cones were marked in an *en face* projection (see Fig. 1(a)). Next, cones were segmented from the volume and their 3D profile (composed of 20 to 25 A-scans) was projected in one lateral dimension, giving cross-sectional (B-scan) images of their reflective surfaces, namely IS/OS and COST (see Fig. 1(b)). Further compression of each cone into a single column of pixels produced an A-scan time trace image (see Fig. 1(c)) — an image in which the vertical dimension represents depth and the horizontal dimension represents time. Both cross-sectional and A-scan time-lapse traces were examined manually for shedding events. For quantitative analysis, the axial positions and intensities of the IS/OS and COST reflections were monitored over time with the IS/OS assigned a nominal position of 0 and the COST position defined in reference to it.

For every cone with a detected disc shedding event, the cone OS length was measured as follows. First, a Gaussian was fit to the intensity profile of the IS/OS and COST reflections of each averaged A-scan following that of Jonnal *et al.* [33]. Axial separation of the peaks of the two Gaussians were measured and defined as the cone OS length. This procedure resulted in 31 OS length measurements per shed cone per 90-minute session. Next, the three contiguous OS length measurements immediately before a gap in COST (manually determined shedding event) were averaged to improve signal-to-noise ratio and likewise the three immediately after. The difference between the two averages was taken as the cone OS length change that resulted from a shedding event.

Finally, the precision to which our method measured changes in the cone OS length was quantified. Twenty-six cones without a detected shedding event were randomly selected from the morning session of Subject #3, and mean and standard deviation of their measured OS length difference were computed across a systematically varied time gap that represented a virtual shedding event. The gap size was increased from 3 to 72 minutes and rolled across the entire session, from which precision was computed.

3. Results

Cone photoreceptors were successfully imaged and tracked in three subjects covering seven 90-minute sessions. 380 cones were analyzed in one session for subject #1, on average 487 cones in each of the three sessions (different days) for subject #2, and 745 cones common to all three sessions (same day) for subject #3.

Figure 1 and Visualization 1 show AO-OCT time-lapse traces of two representative cones in one of the 90-minute imaging sessions for subject #2. Locations of the cones are indicated

Biomedical Optics EXPRESS

by the red and cyan boxes in the Fig. 1(a) image, an *en face* view of the cone mosaic, constructed by registering, averaging, and axial projecting the 31 selected AO-OCT volumes in the session. The *en face* image reveals the lateral extent of the overlap across the 31 volumes. High cone clarity evident in the averaged image confirms the sub-cellular accuracy of our lateral registration method. Time-lapse traces of the reflectance profile of the two cones are shown in Fig. 1(b) cross-sectional and Fig. 1(c) averaged A-scan form as defined in methods. Both views were used to monitor reflectance dynamics of each cone in the 90-minute session. Of relevance here are the bright IS/OS and COST reflections. For the red-labeled cone, IS/OS and COST reflections are evident at all time points and appear axially stable, separated by the same distance (cone OS length) regardless of time point. Average separation was 25.18 μm with a standard deviation of 0.42 μm. These two attributes (stable reflectance and stable axial separation) are the expected appearance of the cone reflection profile based on similar observations in previous AO-OCT cone imaging studies as well as the smooth hyper-reflective banding in the outer retina with conventional OCT [34].The cyan-labeled cone also shows a stable IS/OS reflection, present at all time points, but in contrast shows an abrupt loss of the COST reflection for 18 minutes followed by its abrupt return that is axially displaced anteriorly. Figures 1(d) and 1(e) quantify the OS length change, the difference in length before and after loss of the COST reflection. For this example cone, the OS length decreased from 25.1 μm to 22.7 μm, a difference of 2.4 μm or equivalently a 9.6% loss. For simplicity, we refer to this temporal (loss and return of COST reflection) and spatial (OS length decrease) behavior as a 'COST event,' which we interpret as the optical signature of disc shedding (see Discussion).

The time duration of the loss and return of COST reflection was found to vary considerably, as illustrated by the seven representative cone traces shown in Fig. 2 (top). Duration ranged from less than three minutes (sampling interval of the experiment) up to an extreme case of almost 60 minutes. Frequency of the duration is plotted in Fig. 2 (bottom) histograms for the three morning sessions, one for each subject. Average duration was 8.8 ± 13.4 minutes. Note that abrupt axial displacements of COST reflection without a visible dark gap were counted as disc shedding events. We interpret these as COST events whose duration was rapid (< 3 minutes) and occurred between two successive image acquisitions (3 minutes interval). This scenario is exemplified by the leftmost cone trace in Fig. 2 (top) and contributes to the first bin of the histograms. In some cases, the disappearance of the COST reflection preceded the start of the 90-minute experiment or continued beyond the end of it, e.g., traces denoted with a '*' in Fig. 2 (top). In such cases, we counted the duration to be as long as the portion captured by the experiment, although the actual duration may have been longer and therefore our measurement underestimated the duration. For the cones that fit this scenario, we were unable to measure the OS length change since the beginning or end of the gap was missing in our measurements.

Biomedical Optics EXPRESS

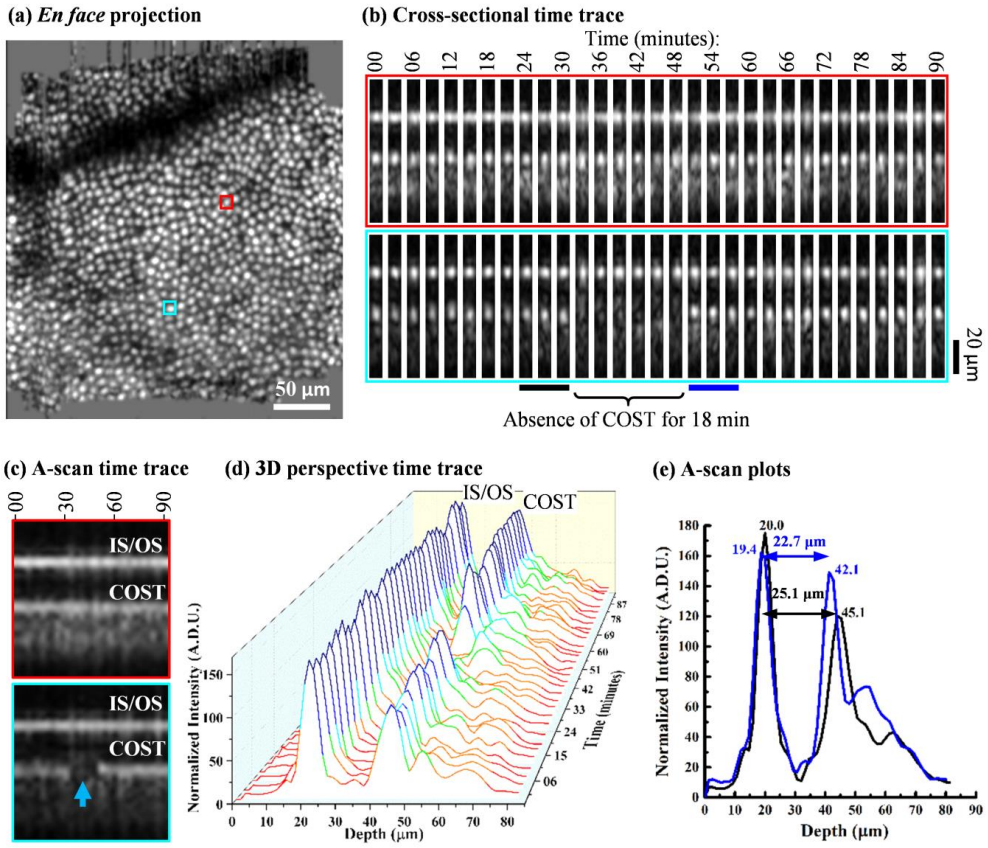

Fig. 1. AO-OCT volume time-lapse traces reveal the optical signature of cone shedding, taken from one 90-minute session on subject #2 (see Visualization 1). (a) Retinal location of the two representative cones are highlighted in red and cyan in the cone mosaic *en face* projection at 3° temporal. The *en face* image is a registered and averaged stack of 31 cone image projections from which the representative cone time traces were extracted. (b) Cross-sectional and (c) averaged A-scan time traces are shown for the two representative cones over 90 minutes. Cross sections are 7 µm wide. The red-labeled trace shows the reflectance profile in which both IS/OS and COST reflections remain visible over the session duration. In contrast the cyan-labeled trace shows an abrupt loss of the COST reflection for 18 minutes (minutes 33 to 51) followed by its return, but axially displaced anteriorly. (d) and (e) quantify the OS shortening of the cyan-labeled cone after the 18 minutes loss of the COST reflection. (d) A-scan time trace is shown on a 3D perspective plot. The black and blue bars highlighted in (b) are the three contiguous time points that immediately precede and follow the temporary loss of the COST reflection, respectively. The average of these contiguous time points are plotted in (e). For this disc shedding event, the OS length decreased from 25.1 µm to 22.7 µm.

Biomedical Optics EXPRESS

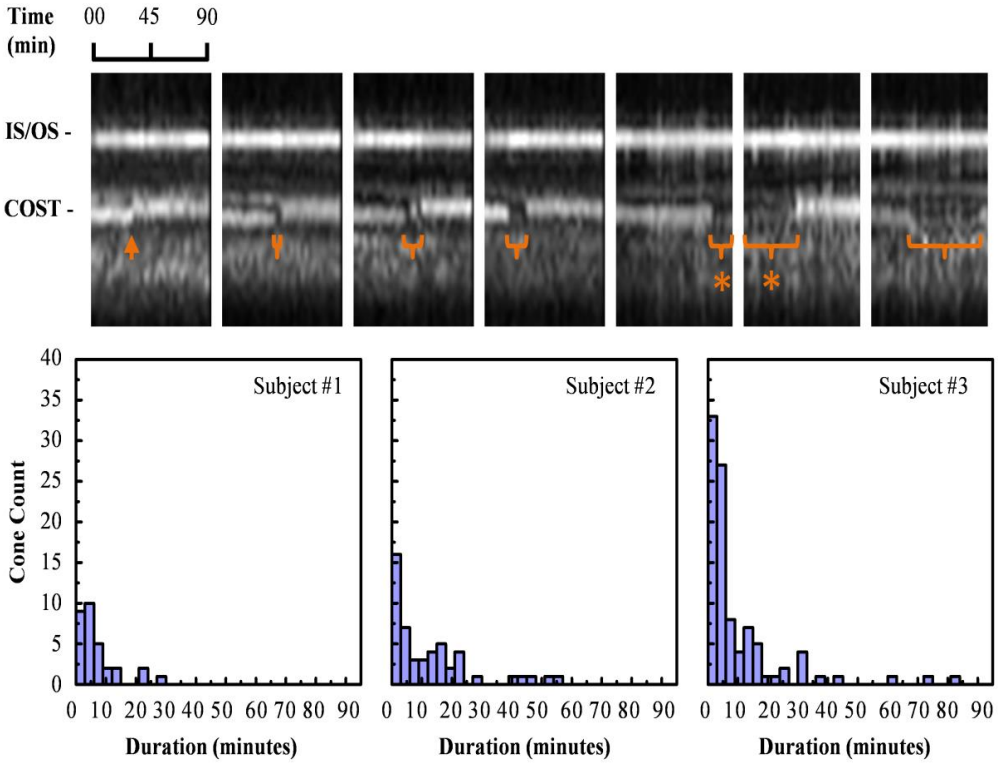

Fig. 2. Temporary loss of the COST reflection varied in duration depending on cone. (top) Averaged A-scan traces of seven cones in the same 90-minute session depict the extent of the variation: < 3, 6, 12, 15, >18, >42, and 57 minutes. For the two cones labeled with asterisks, the loss of the COST reflection initiated or terminated outside the 90 minute duration of the session. (bottom) Histograms summarize the duration frequency of the loss in the COST reflection for cones in the three morning sessions. For loss durations that extended outside the 90-minute session, we counted the duration to be as long as the portion captured by the experiment, although the actual duration may be longer.

We also examined variation of the OS length before and after COST reflectance loss. For this, we compared the Gaussian-fitted IS/OS and COST reflections in the three A-scans that immediately preceded the COST event to the three that followed it using the procedure described in Section 2.3 of Methods. Average peak-to-peak distance between IS/OS and COST in the Gaussian-fitted A-scans was the OS length, and the difference between the two (before and after the COST event) was defined as the OS length change. Results are shown in the Fig. 3 histograms for the three morning sessions. In all cases observed, the OS length decreased. Note though that when the length change was too small to be resolved by our system (empirically determined to be <0.4 μm, see Discussion), we included it in the first bin in the histograms. For subjects #1, #2, and #3, the average decrease of OS length (computed for each cone, then averaged) was 2.5 ± 1.0 μm, 1.6 ± 1.2 μm, and 2.2 ± 1.0 μm, respectively. The corresponding percent decrease (computed relative to each cone's own length, then averaged) was 7.9 ± 3.1%, 6.0 ± 4.4%, and 7.1 ± 3.2%. For reference, the average OS length before loss in the COST reflection was 31.6 ± 1.5 μm, 25.5 ± 1.7 μm, and 30.9 ± 1.8 μm for subjects #1, #2, and #3, respectively.

We assessed two additional properties of the COST events: their spatial arrangement in the cone mosaic and their frequency as a function of time of day (morning, afternoon, and evening). Figure 4 images and plots capture both parameters using the three imaging sessions for subjects #2 and #3. Yellow, green and magenta dots mark the spatial locations of cones

Biomedical Optics EXPRESS

that exhibited a COST event in their respective imaging sessions. For subject #2, these events correspond to 14.5%, 6.4%, and 4.0% of the total cones (386, 451, and 623) that were registered and tracked in each session. For subject #3, these events correspond to 14.1%, 5.0%, and 4.0% of the total 745 cones that were registered and tracked across the three sessions. To better assess spatial arrangement of the COST events across the day and the low percentage of cells that showed more than one COST event on the same day, Fig. 5 superimposes the color coded COST events in Fig. 4 for subject #3 on one background. Different markers were used for cones with more than one COST event. The figure contains an additional panel that marks all tracked cones and facilitates assessment of the impact of untracked cones on the distribution appearance of COST events, as for example in the shadow of a blood vessel where cones could not be tracked.

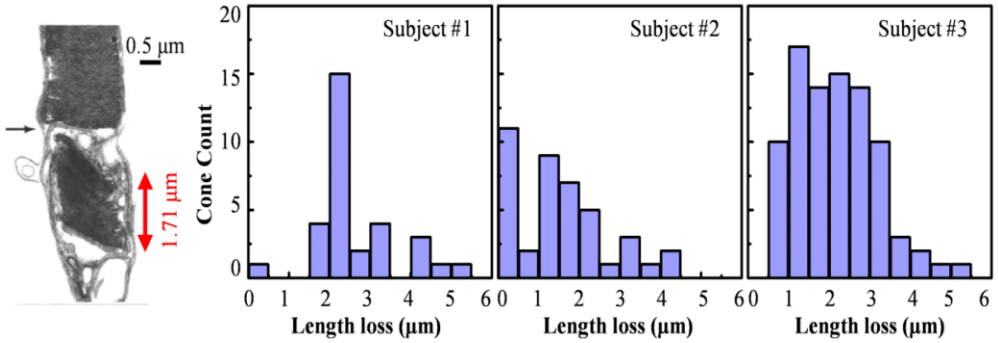

Fig. 3. Temporary loss of the COST reflection was accompanied by a small decrease in the OS length. Histograms show the frequency of the length change for the three subjects in their morning sessions. For comparison, histologic cross section obtained on human depicts a shed disc packet at the OS posterior tip of a cone photoreceptor [13].

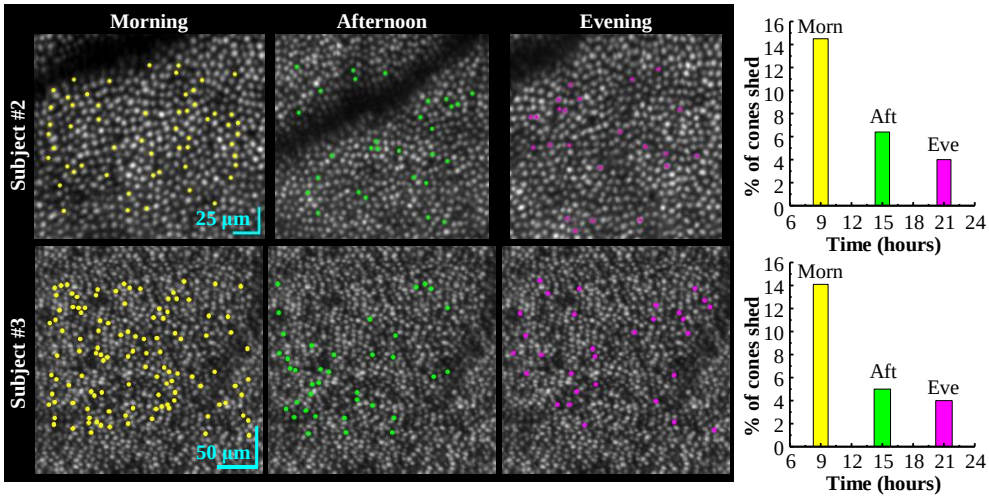

Fig. 4. Spatial pattern of COST events during each 90-minute imaging session (morning, afternoon, and evening) for two subjects. The *en face* AO-OCT images are registered and averaged stacks of 31 cone images, one at each time point in the imaging session. Clarity of the cone mosaic substantiates the sub-cellular registration. Detected COST events are color coded and superimposed above the corresponding cone in the *en face* AO-OCT images: yellow (morning), green (afternoon) and magenta (evening). Note difference in scale bars for the two subjects. The bar plots show the percentage of tracked cones that were identified as undergoing a COST event during one of the three imaging sessions: morning, afternoon, and evening.

Biomedical Optics EXPRESS

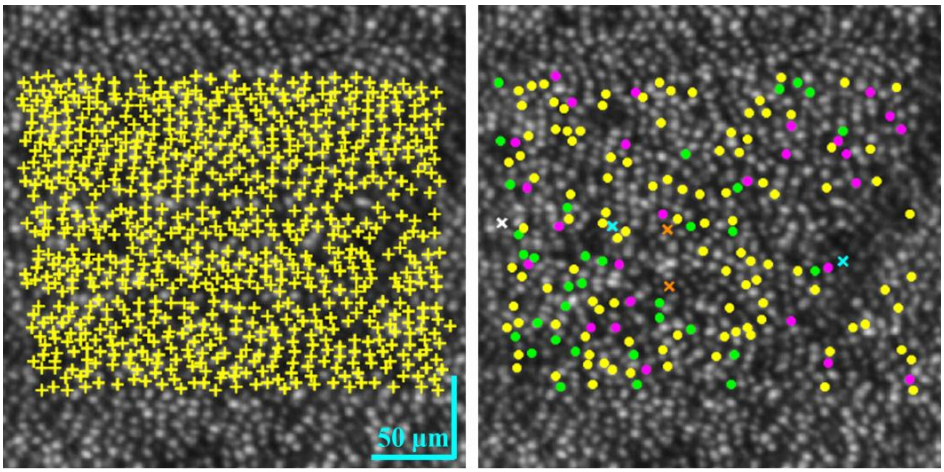

Fig. 5. Spatial pattern of the 745 tracked cones and 175 detected COST events for the three 90-minute imaging sessions of Subject #3. (left) Tracked cones, common to all three sessions, are superimposed with yellow ' + ' markers in the *en face* AO-OCT image. Cones that exhibited a single COST event are superimposed with solid circles color coded as yellow (morning), green (afternoon), and magenta (evening). The five cones that exhibited two COST events are superimposed with ' × ' markers color coded as cyan (morning & afternoon), orange (morning & evening), and white (afternoon & evening).

4. Discussion

In this study we took advantage of the sub-cellular 3D resolution of AO-OCT and sub-cellular 3D registration, both developed in our laboratory, to investigate local dynamics in the reflection of individual cones. We successfully isolated and tracked over hours the IS/OS and COST reflections of thousands of cones in three subjects, yielding time-lapse images sampled every three minutes. What we observed – much to our surprise – was that a small but notable fraction of the cones underwent an abrupt, transient loss in their COST reflection followed by a slight decrease in the cone OS length. We know of no previous report of such change even though cone photoreceptors generate some of the brightest reflections in the retina and are the most studied retinal cell using high-resolution retinal imaging systems, including OCT and other modalities assisted with AO. In addition, clinical OCT is routinely used to assess health of cone photoreceptors by analyzing the outer retinal bands in the OCT images. Despite this plethora of imaging, we found that to detect these isolated, sub-cellular occurrences required additional imaging capability as used here.

Three points warrant discussion: (1) the ability of our method to track individual cones with sufficient spatial and temporal resolution to detect cone shedding events; (2) properties of disc shedding, specifically optical signature, time of occurrence, and load distribution; and (3) the origin of the COST reflection.

4.1. Tracking individual cones in 4D

Fundamental to our method is the ability to track in all three dimensions the IS/OS and COST reflections of individual cones over hours. Clear individuation of cones in the averaged *en face* images, as for example Figs. 1(a), 4, and 5, provide qualitative evidence that the volumes acquired over the imaging sessions were registered in XY with an accuracy much better than the row-to-row spacing of cone photoreceptors (~6.3 µm). To confirm tracking, we visually inspected the time trace of individual cones that exhibited COST events to assure cones were correctly located at each time point and not mislabeled by registration. Furthermore, the central core of the strip-based registration method used here was validated for cone imaging in several of our prior AO-OCT publications [19, 31, 32], although for different imaging protocols and study objectives.

Biomedical Optics EXPRESS

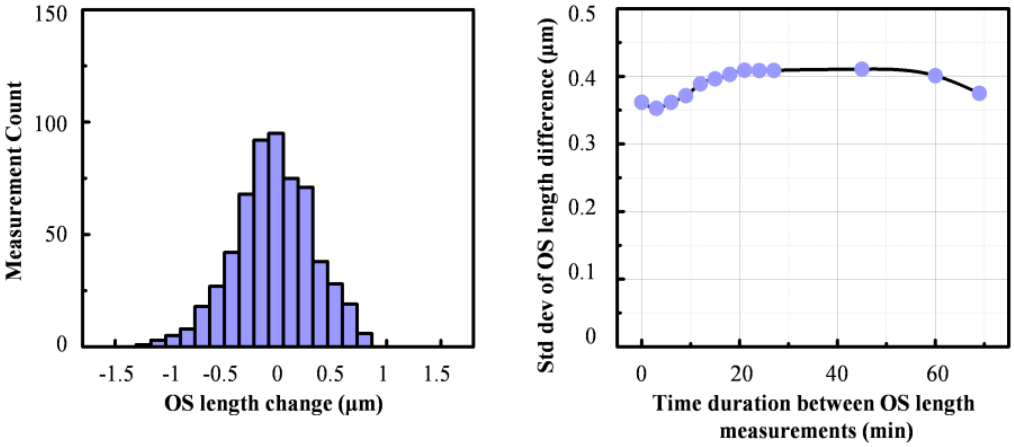

Fig. 6. Measurement precision of cone OS length changes as a function of time interval between measurements. Measurements were obtained on 26 non-shedding cones in the morning session of Subject #3. (left) Representative histogram of OS length change shows a Gaussian-like distribution centered about zero and with a standard deviation of 0.37 μm. Histogram is for a time interval of 9 minutes, selected because it approximates the average duration of the COST event (8.8 ± 13.4 minutes). (right) Standard deviation of OS length differences is plotted for all time intervals considered (0 to 72 minutes).

More critical is axial registration and the measurement of cone OS length. For the three subjects of this study, our measurements showed an average OS length decrease of 2.1 μm following a COST event, which is a factor two smaller than the 4.2 μm nominal axial resolution of our AO-OCT system. While resolution is important, it does not define the limit to which an axial motion can be measured, which one may describe as a problem of localization rather than resolution. In our case OS length changes were based on averages across 20-25 A-scans per cone, three contiguous time points before and after the COST event, and Gaussian fits of the IS/OS and COST intensity profile. Using this method, we quantified the precision to which changes in OS length could be measured as a function of the COST event duration (see Fig. 6). As shown, standard deviation of the change is ~0.4 μm and insensitive to the time interval (0 to 72 minutes) between OS length measurements. This precision is almost 6× better than the average OS length change of 2.1 μm, confirming we indeed achieved the necessary precision to detect individual disc shedding events.

4.2. Optical signature of cone disc shedding

Imaging cone photoreceptors in three normal subjects, we observed two key optical signatures of the COST event: time duration of the event (loss and return of the COST reflection) and reduction in cone OS length. We attribute these changes to OS disc shedding on several grounds articulated below and in addition that we know of no other physiological phenomena in the photoreceptor terminal that could cause such a marked, transient change in both reflectance and length of the OS and that occurs so rarely for any given cone.

As examined in Fig. 2, average duration of the COST event was 8.8 minutes, but varied considerably between cones (standard deviation = ± 13.4 minutes) with the most frequent duration being < 3 minutes. We were surprised how dramatic the loss in the COST reflection was for most cones, resulting in what appeared to be a complete loss of COST reflection in the AO-OCT cone cross sections. We had originally thought that the optical signature of disc shedding might include multiple axial reflections or an axially extended reflection at the OS posterior tip due to possible refractive index mismatches at opposing ends of the detached disc packet with the surrounding cytoplasm of the RPE apical processes. While some COST events showed suggestive evidence of multiple reflections, example Fig. 2 (top row, 2nd from left cross section), the vast majority did not and we did not find evidence of reflections that

Biomedical Optics EXPRESS

descend the RPE apical processes, which would follow the expected route of the disc packet as it is phagocytized by the RPE cell. One possible explanation for the lack of additional reflections is that disc packets have been reported to rotate 90° as they descend [13]. This rotation coupled with evidence that the COST reflection is specular [30] could redirect the packet reflection out of the cone OS, causing the packet to appear invisible to AO-OCT.

Rotation, however, cannot explain the initial lack of reflection at the new terminal end of the OS, which forms when the packet separates from the OS. The first stage of disc shedding involves cleavage of terminal discs by the RPE membrane, a physiological process that must disrupt the OS terminal interface as discs that define the original interface are discarded and replaced with new ones. But whatever anatomical changes occur during the cleaving, our AO-OCT measurements indicate these changes have a profound effect on the reflective properties of this interface, at least temporarily. Perhaps cleaving initially leaves the terminal end optically rough causing the reflected light to scatter over a broad range of angles and little re-captured by the overlying cone. Alternatively, cleaving may form a temporary gradation in index of refraction that lets most of the light propagate deeper without scatter. Regardless of what the mechanism is, the effect is temporary with a new COST reflection eventually emerging and signifying the end of the COST event. Another puzzle is why the recovery takes almost 10 minutes on average and varies so much between cones, from <3 minutes to hours. Clearly more work is needed to identify the underlying anatomical and physiological mechanisms that account for these aspects of the COST event.

The second key optical signature of the COST event is shortening of the cone OS length as examined in Fig. 3. Across the three subjects imaged, the COST event resulted in an average OS length decrease of 2.1 ± 1.1 µm. While it has not previously been possible to measure disc shedding in living animals, let alone humans, numerous *ex vivo* studies based on electron microscopy have been conducted to study the size of phagosomes in the RPE cells underlying the cone OS in mammals. Reported sizes include 1.6 µm in the squirrel [16], 1.15 µm in the domestic cat [35], and 1 to 3.23 µm in the Rhesus monkey [13, 36]. Another metric for comparison is daily renewal rate, the continuous assembly of new membranous discs at the proximal end of the OS, a slow process that increases OS length. In order to maintain a constant OS length, daily renewal rate must equal the size of the disc packet shed, assuming each cone sheds once daily. Renewal in the living human retina has been reported to add 2.2-2.7 µm [17], 3.6 µm [19], and 2.6 µm [18] to the OS length over a day. Furthermore, in *ex vivo* studies of mammalian rods, daily renewal rates have been reported to be 1.8 to 2.2 µm/day in mice [12, 37, 38], 1.8 to 2 µm/day in dogs [39, 40], and 2.6 to 2.8 µm/day in rhesus monkeys [41]. Our report of cone OS length shortening (2.1 ± 1.1 µm) falls within the range of both estimates, daily disc shedding and renewal rates, further evidence that our method is measuring disc shedding.

4.3. Time of occurrence

We counted the number of COST events in each of three 90-minute sessions (morning, afternoon, and evening) in two subjects to determine if occurrence was influenced by time of day. Figure 4 summarizes our findings and shows similar trends of occurrence for both subjects. COST events were observed in all 90-minute sessions, but with frequency notably elevated in the morning and decreasing monotonically with each subsequent session. Averaged across the two subjects, percent of total tracked cones that exhibited a COST event was 14.3% (morning), 5.7% (afternoon), and 4.0% (evening). The relatively low percentage of tracked cones that experienced a COST event during the three imaging sessions was just 24% (= 14.3% + 5.7% + 4.0%), raising the question as to why so many (76%) did not. It is likely that these other cones may have, but went undetected as our three 90-minute sessions sampled only a small fraction (~19%) of an entire day (24 hr), leaving considerable time for COST events to occur at times we did not monitor. As a hypothetical example, if COST events occurred over the entire day at the average rate we measured (5.4%/hr for the three 90-

Biomedical Optics EXPRESS

minute sessions), all cones would experience a COST event in 18.5 hr, 5.5 hr less than a 24-hour day and fulfilling the generally held requirement that cones should shed daily.

Both the elevated COST events in the morning (14.3%) and reduced, but nonzero, COST events in the afternoon (5.7%) and evening (4.0%) sessions present an intriguing view of when human cones shed during the day, a longstanding unknown. To put in perspective, photoreceptor renewal and shedding have been extensively studied in animal models in postmortem eyes since first discovered in rods by Young in the late 1960s using radioactive amino acids [11, 12] and then later in cones [13–16]. Rod photoreceptors have been demonstrated to have a highly conserved diurnal rhythm of shedding [42–46] when under cyclic lighting conditions, a process found to be regulated by circadian influence [47–49]. Numerous species have been examined for rod shedding (goldfish [44], frog [50], rat [49], mouse, chicken [43], cat [42], and rhesus monkey [36]) and all have demonstrated shedding that occurs in a diurnal burst shortly after light onset and regulated by light changes and circadian effects. Cone shedding – while studied much less extensively than rods – has proven similar to rod shedding, a diurnal rhythm in all instances studied. However unlike rod shedding, the timing for cones varies widely among species. Peak cone shedding was found to occur after light onset for the Nrl knockout mouse [51], Nile rat [52], tree shrew [53], and cat [42], and after dark onset for goldfish [44, 54], lizards [45], chicken [43], tree squirrel [55], ground squirrel [56], and rhesus monkey [36]. Clearly missing from these two lists are humans, which our results begin to elucidate. Interestingly, unlike that of the rhesus monkey (the closest species to human examined [36]), our results point to a peak after light onset (not dark onset), with the additional surprise of low-level shedding throughout the period of light. Clearly more experiments are needed to validate these early findings and to examine the influence of light changes and circadian effects. This work is in progress.

As previously noted, the longstanding view is that cone photoreceptors shed only once per day. Our results provide some insight into this assumption. For the 745 cones tracked and evaluated in Subject #3 across the morning, afternoon, and evening sessions, only five cones were found to have two COST events and none showed more. The 0.7% incident of multiply-shed cones likely lies within our measurement error to detect COST events and supports the premise that cones shed daily.

4.4. RPE load distribution

RPE cells phagocytose an immense amount of photoreceptor material over their lifetime. Because these cells are post-mitotic, efficiency in phagocytosis is critical for preventing accumulation of damaging waste byproducts and the consequence of degenerative eye disease. RPE load distribution may play a fundamental role in their efficiency as each RPE cell services multiple cones (and rods), all of which presumably shed each day. That is, efficiency may dictate that shedding is spatially and temporally distributed to match the grain of the RPE cell mosaic thereby avoiding the heavy demand of a single RPE cell to phagocytose all of its connected cones at once.

We know of no reports in the literature that have measured the distribution of shedding across the retina (regardless of animal model), perhaps because it requires tracking cells over time, which is not possible with postmortem eyes and requires individuating both cones and RPE cells. While our results are preliminary, the *en face* images in Figs. 4 and 5 show little evidence of clustering of COST events, suggesting shedding is spread across the cone patch, a necessary requirement if shedding is to match the grain of the RPE mosaic. A correct test of this hypothesis requires mapping of cones to RPE cells, which we did not do in this study, but is now possible using further advances we have made with our AO-OCT-based method as validated by Liu *et al.* (2016) [32].

That COST events do not appear clustered may also provide insight into the mechanism that initiates shedding. Recent evidence by Ruggiero, *et al.* (2012) [57] using a mouse model points to the exposure of phosphatidylserine (PS) at the posterior end tips of rods as an “eat-

Biomedical Optics EXPRESS

me" signal that initiates shedding. But loss of either the phagocytosis receptor αvβ5 integrin, expressed by the RPE but not by photoreceptors, or its extracellular ligand milk fat globule-EGF factor 8 (MFG-E8) are necessary for PS exposure to occur. Thus RPE appears to play a central role in initiating shedding. This result combined with the lack of clustering in our own data points to the intriguing possibility that RPE cells are able to control shedding on an individual cone basis.

4.5 Attribution of COST reflection

The COST reflection is central to our investigation of disc shedding; yet there remains some disagreement in the literature over the attribution of this reflection, an issue recently summarized by Jonnal, *et al.* (2014) (see *Band 3* subsection in *Discussion*) [33]. This disagreement is in part due to the fact that clinical OCT sometimes has difficulty separating the COST band from the underlying reflections in the RPE layer – especially in the fovea – and more importantly shows COST with a thickness greater than would be expected from a reflection at the distal tip of the cone OS. Because of this, the COST reflection was termed the "interdigitation zone," with the term "zone" indicating the lack of evidence for a specific reflective structure, e.g., COST, by the International Nomenclature for Optical Coherence Tomography Panel [58]. AO-OCT does not share the imaging limitations of clinical OCT and acquires sharper images in all three dimensions, in this case showing clear separation of the COST reflection from not only those above and below it, but also those laterally on the scale of individual cone cells. As a result, individual cones are observed and exhibit a COST reflection whose axial thickness approaches the axial resolution of our AO-OCT system, indicative of a highly localized reflection. Consistent with previous AO-OCT reports, this reflection was attributed to COST here. Our disc shedding results themselves provide further support of a COST attribution. We know of no other physiological mechanism at this depth in the retina that could cause such an abrupt, transient, highly localized, and rarely occurring change in reflectance, other than a shedding event, which is known to occur at COST based on considerable histologic evidence.

Finally, attribution differences between clinical OCT and AO-OCT studies are becoming increasingly common and not limited to the COST reflection. For example, our recent AO-OCT study of the 3D reflectance profile of the "RPE/Bruch's complex" band (as recognized by the International Nomenclature for Optical Coherence Tomography Panel [58]) showed this band to be more complicated, composed of multiple hyper and hyporeflective sublayers. We observed two hyperreflective sub-layers that we identified as rod outer segment tip (ROST) and RPE and sometimes a third that we attributed to Bruch's membrane [32].

5. Conclusion

We report discovery of the optical signature of cone OS disc shedding, measured using a novel method based on AO-OCT in conjunction with post processing to track and monitor individual cone cells in 4D. Using this optical signature, we measured the temporal and spatial properties of shedding events in three normal subjects and established a clear path for future studies of disc shedding in the living retina. To the best of our knowledge these are the first images of photoreceptor disc shedding in the living retina.

Funding

This study was supported by National Eye Institute grants R01-EY018339, K99-EY026068 and P30-EY019008.

Acknowledgments

We thank William Monette and Thomas Kemerly for machining and electronic support.